Time-averaged and time-varying plasma potential in the near-field plume of a Hall thruster.

IEPC-2013-214

Presented at the 33^{rd} International Electric Propulsion Conference,
The George Washington University, Washington, D.C., USA
October 6–10, 2013

A. Pétin* and S. Mazouffre
ICARE, CNRS, 1c avenue de la recherche scientifique, 45071 Orléans, France.

K. Dannenmayer
ESTEC, Keplerlaan 1, 2201 AZ Noordwijk, Netherlands

and

P. Kudrna and M. Tichý
Charles University, Faculty of Mathematics and Physics, Prague, Czech Republic.

Time-averaged as well as time-resolved measurements of the plasma potential have been performed in the near-field plume of a low power Hall thruster by means of an emissive probe. A fast linear drive has been used to leave the emissive probe only for a short time in the plasma. A system to probe high frequency oscillations of the potential up to ~1 MHz has been developed and tested. Several measurements in the near-field plume are presented and discussed.

Nomenclature

B	= magnetic field (G)
e	= elementary charge (C)
E	= electric field (V/mm)
E_x	= x component of the electric field (V/mm)
E_y	= y component of the electric field (V/mm)
I_d	= discharge current (A)
$\dot{m}_{Xe}$	= mass flow rate (Xenon) (mg/s)
n_e	= electron density (cm^{-3})
p	= pressure (mbar)
T_e	= electron temperature (eV)
U_d	= discharge voltage (V)
V_{crp}	= cathode to ground potential (V)
V_f	= floating potential (V)
V_p	= plasma potential (V)

*PhD student, ICARE, CNRS, France, aude.petin@cnrs-orleans.fr

I. Introduction

A Hall thruster (HT) is one type of electric engine currently in use onboard geosynchronous satellites. One scientific space probe had used a HT (SMART1). In a HT, a low pressure ExB discharge is generated. Since only electrons are sensitive to B, a charge separation appears and increases E which is at the origin of the ion acceleration [Dannenmayer and Mazouffre, 2011]. As no grid assembly is employed for beam generation, such a thruster is not current limited and a relatively large thrust level, in comparison with gridded ion engines, is achieved. The thrust-to-power ratio of HTs is higher than for gridded ion engines. The high specific impulse (I_{sp}) compared to chemical propulsion devices makes this technology of great interest for orbit transfer maneuvers, end-of-life deorbiting and deep-space exploration missions. An important issue in the field of electric propulsion is the interaction between the host spacecraft and the plasma plume. A large amount of studies were performed on ion flow properties. Recently we carried out time-averaged and time-resolved measurements of the electron density n_e and temperature T_e as well as plasma potential V_p in the plume of several Hall Thrusters by means of Langmuir and emissive probes [Dannenmayer et al., 2012] and [Dannenmayer and Mazouffre, 2013]. One of the objectives was to provide accurate data for validation of plasma plume numerical simulations. Another critical point for understanding the complex physical mechanisms at work in the discharge of a Hall thruster is the electron cross-field diffusion and its relationship with plasma-surface interactions. A thorough knowledge on the plasma structure in terms of electron parameters is therefore required. Furthermore, the discharge of a HT is strongly non-stationary with plasma oscillations and fluctuations ranging form a few kHz up to a few GHz.

In this contribution we present time-averaged measurements of the plasma potential V_p in the near-field of a low-power permanent magnet HT. We also present preliminary time-resolved measurements of V_p in the near-field plume with a frequency resolution above 1 MHz.

II. Experimental setup

A. Thruster and Vaccum facility

Experiments discussed in this paper have been performed with the PPI thruster of ICARE laboratory [Mazouffre et al., 2012]. The PPI is shown in Fig. 1. This low-power thruster (typically 200 W) has four specificities: (1) coils are substituted by permanent magnets (SmCo) set up on two iron rings on either sides of the channel. A soft iron piece conducts magnetic lines to obtain the wanted magnetic topology; (2) the gas is injected through a porous ceramic ring which increases gas homogeneity; (3) the thruster is equipped with copper heat pipes decreasing thruster heat and avoiding to reach Curie point; (4) three channel geometries, corresponding to three channel widths, are possible. In this paper, experiments have been performed with the medium channel geometry: the channel width is 1 cm. Finally, two types of channel ceramics are used: Al_20_3 and $BNSi0_2$.

All experiments discussed in this article were performed in the NExET chamber (New Experiments on Electric Thruster). This is a cylindrical chamber of dimensions 1.8 m in length and 0.8 m in diameter. Its three pumping stages (primary, turbo molecular and cryogenic) permit to reach a chamber pressure of approximately 8.10^{-5} mbar-N_2. The mass flow rate of Xenon through the gas injector was 1 mg/s during all experiments. The cathode gas flow rate was kept fixed at 0.2 mg/s.

B. Emissive probe and piezo-electric stage

All measurements described in the present paper have been obtained with an emissive probe. This emissive probe is composed of a 0.15 mm diameter thoriated tungsten wire inserted into two juxtaposed copper wires. The free tungsten length is 5 mm. These two layers of copper wires are visible in Fig. 2 (left). Then, the copper wires are stuck into a 4 mm diameter alumina tube (bottom of the picture). The method of the floating point [Sheehan and Hershkowitz, 2011] is used to get the plasma potential: the potential of a sufficiently heated probe corresponds to the plasma potential. Figure 2 (right) shows a heating curve of the emissive probe. The floating potential of the probe increases with the heating current until it reaches saturation. At saturation, we can consider that the probe emits enough electrons to cancel out its sheath and then, its floating potential is equal to the plasma potential. According to the the Orbital Motion Limited (OML) theory, the electron temperature is obtained thanks to the relation (case of xenon plasma) [Smith and Cappelli, 2010]:

$$T_e = 0.1897(V_p - V_f) \tag{1}$$

where V_f is the floating potential of the cold probe. The electric field is deduced from the plasma potential using:

$$\vec{E} = -\vec{\nabla} V_p \tag{2}$$

The accuracy associated to the emissive probe is of the order of $T_{heating}/e$, with $T_{heating}$ the heating temperature of the tungsten wire, but the error is generally larger. Even if a surface has a high emission, its potential is T_e/e times lower than the plasma potential. That is a drawback of emissive probes in high electron temperature plasmas [Sheehan and Hershkowitz, 2011]. Then, Langmuir probe measurements will be necessary to complete these first measurements.

The high particles flux in the near-field plasma strongly decreases the lifetime of the probe. The measurements were then performed thanks to a fast-moving stage. This stage is the PILine® Linear Motor Stage M664K018. This linear drive reaches a maximum velocity of 350 mm/s and maximum acceleration and deceleration of 2000 mm/s^2. Its dimensions are 140 × 63 × 14 mm^3. A picture is shown in Fig. 3. The linear stage has a travel range of 90 mm (45 mm on both side) and furthermore, it is vacuum compatible down to 10^{-6} mbar. This piezo stage was already presented in literature [Dannenmayer and Mazouffre, 2012].

The main configuration of the probe during the experiments is shown in Fig. 4 "config. 1". The probe was placed parallel to the thruster axis to minimize the disturbance due to the alumina tube sputtering. The thruster was mounted up on a X-direction movable stage. The probe was fixed on the piezo stage and move in the Y-direction. An oscilloscope recorded the probe signal during an Y-direction trip of the probe for each X-position of the thruster.

An other configuration has been tested with the purpose to perform measurements in the plasma inside the thruster channel. The probe is moved in the X-direction thanks to the piezo stage. This configuration is showed in Fig. 4 probe "config. 2". These two configurations are discussed in the following section.

III. Time-averaged measurements

A. Measurement description

The first probe configuration was used to obtain contour plots of V_p, V_f, T_e, E_x, E_y in the near-field plasma. The thruster operating parameters are U_d=200V, I_d=0.93-0.94 A, $\dot{m}_{Xe}$=1 mg/s and the pressure is p=1.2.10^{-4} mbar-N$_2$. V_f, V_p, I_d and V_{crp} have been recorded with a time resolution of 20 ms. In the following figures, Yn correspond to the Y-direction normalized by the channel radius: Yn=Y/r_c with the channel mean radius r_c=18.5 mm.

The plasma potential, which is, in the case of our emissive probe, the floating potential of the probe heated with 4.4 A current, is shown in Fig. 5. It presents an axial symmetry and the maximum intensity (V_p=70 V) is reached on the channel axis close to exit plane. The plasma potential decreases very quickly on the channel axis, moving away from the thruster. An other lower maximum is obtained on the thruster axis, which is more visible on the profile as a function of the distance from the thruster (Fig. 9).

The electric field can be computed from the plasma potential. The contour plots of the X and Y components are plotted respectively in Fig. 6 and the profile of the X component on the channel and thruster axis is visible in the Fig. 9. On the thruster axis, E_x is directed toward the thruster, only at the exit plane. This is due to the sheath close to the thruster face and that induces the sputtering of this area by ions. On the channel axis, E_x decreases strongly with the distance from the thruster exit plane.

The floating potential, which is the potential of the cold probe, is shown in Fig. 7. There are two maxima of same intensity (V_f=8 V): one on the channel axis, close to the exit plane; another one farther from the thruster on the thruster axis. This is also visible on the profile of V_f, in Fig. 9.

The electron temperature is shown in Fig. 8. The maximum intensity (T_e=11 eV) is reached on the channel axis near the exit plan. On the thruster axis, T_e reaches 6 eV.

V_p, V_f, T_e contour plots have already been performed in an other 200 W Hall thruster, in near-field, with an emissive probe [Smith and Cappelli, 2010]. Several differences and similitudes appear. In this previous paper, mainly, on either sides of the thruster axis, the plasma potential reached higher values and showed two symmetrical maxima. The floating potential did not reach a maximum on the channel axis, contrarily to our data. The electron temperature showed a much more complex structure. However, despite the different intensity of the floating and plasma potential on the channel axis, the resulting electron temperature is the same, i.e., about 10 eV. Discrepancies could be due to a different magnetic configuration.

The second probe configuration permits to obtain several profiles of V_p, V_f, T_e versus X-direction. These measurements have been performed for three voltages: 150, 200, 250 V, on the channel axis. While the channel ceramic of the thruster was Al_20_3 for the first configuration, it was $BNSi0_2$ for the second configuration. Profiles are presented in Fig. 10 and the profile in the first configuration is also plotted, for comparison. The gradient of V_p and T_e is sharper in Al_20_3 than in $BNSi0_2$. An increase of the discharge voltage is associated to an increase of V_p and T_e. The behavior of the floating potential is interesting. There is a trough at about 3 mm in front of the exit plan. This decay is not easily associated to the potential. It is necessary to do more measurements before to conclude about it.

B. Measurement accuracy

1. Procedure

The probe senses two kind of plasma variations: spatial variations due to the probe motion, and time variations due to the oscillation of the plasma. We can consider only two main plasma oscillations: the Breathing Mode (BM) (∼18 kHz) and the Ion Transit time ITT (100-400 kHz). Two criteria must be followed:

1. During one breathing oscillation time period, the length travelled by the probe must be less than L_g, with L_g the gradient length (BM period as it is the longest time scale of interest here). Then $v_{probe}T_{BM} \ll L_g$.
2. The time resolution of the acquisition system must be much below the shortest period. We are interested in probing the transit time oscillations with a frequencies up to 1 MHz. Thereby $\Delta t \ll 1/f_{maxITT} \approx 1\mu s$

Finally, our recording permits to have 12 $T_{f_{min}}$(and more than 260 $T_{f_{max}}$) during the time when the probe is considered motionless but our resolution is not high enough and will be increased in the future experiments.

2. Disturbance due to the probe

As long as measurements are performed far from the thruster, in low plasma flux areas, disturbances of the plasma due to the probe are negligible. However, near the thruster, the probe is strongly sputtered. Figure 12 gives the discharge current and the cathode potential for several distances of the probe from the thruster, during a trip of the probe in front of the thruster (probe configuration 1). Both cases of heated probe and cold probe are shown. The measurements have been performed with a sample length of 30000 points. The processing consisted in averaging over 500 points. The probe was installed on the piezoelectric stage and its velocity in function of the Y-direction is given in Fig. 11 (left-hand side). Observed disturbances are: (1) disturbances due to the alumina tube sputtering, (2) disturbances due to the heating of the probe (either directly from tungsten, or from a higher sputtering of the alumina tube). Figure 12 shows that the perturbations increase gradually when the probe moves closer to the thruster. A heated probe perturbs more than a cold probe. A cold probe starts to disturb the plasma at a little bit more than 13 mm from the exit plane whereas a heated probe already disturbs at 20 mm. On the channel and thruster axes, disruptions are higher, perhaps due to a higher sputtering in these areas. Actually, the highest disturbance occurs at Yn $= -1.25$, i.e., where the the probe starts to penetrate the beam. In a surprising way, near the exit plane, and far away from the thruster and channel axis (Yn < -2.5, i.e., before the trip in front of the thruster) a heated probe disrupts less than a cold probe. Finally, the maximum disturbance (Yn $= -1.25$, close to the thruster), the perturbation on I_d is about 10 % and on V_{crp} about 30 %. Disturbances described above correspond to an increase of I_d and a decrease of V_{crp}. The sputtering of alumina tube increases I_d. To keep charge neutrality, the cathode emits more electrons by decreasing of its potential. When the probe is heated and emits electrons, we can also understand an increase of I_d but not the decrease of V_{crp}. Then it is possible that the sputtering of the tube increase when the probe is heated.

I_d and V_{crp} for both probe configurations are compared in Fig. 13. It is important to notice that the channel ceramic also changes between each probe configuration. Surprisingly, the change of I_d and V_{crp} induced by the probe moving inside the thruster is not so high. This is all the more surprising that the probe needs to decelerate and stops inside the channel (see Fig. 11, right-hand side). We expected to obtain a much higher sputtering. However, the probe stops at 1 mm to the exit plane inside the channel, then it is possible that the disturbance still increases when the probe move farther inside. Finally, Figure 13 shows that the behavior of I_d in the two configurations is similar, independently from the thruster power and the channel ceramic. The behavior of V_{crp} presents, in the first configuration, several peaks distributed each 10 mm. These peaks are sharp and then certainly not physical, but due to a problem in our set up.

IV. Time-resolved measurements

A. Probe electrical circuit

Emissive probes used with the "floating point method" have the advantage to give directly a time-resolved measurement of V_p. Indeed, no sweep of the probe voltage is required, as for Langmuir probe. However, the power supply necessary for heating represents unavoidable capacity to the ground (C) which together with the resistance of the probe (R) form a low-pass filter with a cutoff $f_{cut} = (2\pi RC)^{-1}$. In order to observe high frequency plasma oscillations (such as ITT) either C or R have to be reduced. Several ideas have been tested:

1. The equivalent capacity C of the heating power supply can be decreased connecting the power supply to an insulation transformer or to an Uninterruptible Power Supply (UPS) which is powered by batteries only.

2. Decrease the effective resistance of the probe, especially for higher frequencies, using the active part – AC voltage follower.

3. The third idea was to separate the heating power supply capacitance from the emissive probe by inserting serial impedance in between. Because the heating circuit is symmetric, two coils of the toroidal transformer are inserted symmetrically in series with each pole of the heating power supply. The polarity is chosen in such a way that the magnetic fluxes from the symmetric heating current cancels each other and represent negligible impedance while for the asymmetric (common mode) currents from plasma oscillations the full coils inductance of 2 mH applies. To intensify the effect we used 5 coils in series.

4. We finally tried to mix these ideas.

Figure 14 (top) illustrates the main tested circuits. Figure 14 (bottom) shows the measured transfer functions for these circuits and for some others which are easy to derive from the main ones. Some transfer function presents a resonance peak which comes from possible parasitic capacities. The main purpose was to avoid a resonance in an frequency range of plasma oscillations. We can see in Fig. 14 that the simple case, i.e., only the heating circuit floating (via an insulator) and the oscilloscope (green/up triangle) presents two problems at high frequency: an attenuation of the signal and a resonance frequency. The same simple circuit using a battery (UPS) to make the heating circuit floating (purple left triangle) permits to avoid the attenuation but there is still a resonance frequency. These transfer functions have been obtained considering the probe as a signal generator and a resistance in series. We used a resistance of 1 kΩ since this is the highest probe resistance measured in the plasma (near the exit plane where the flux is high). Actually, since the probe resistance changes as function of plasma flux, this resonance frequency can be shifted during the measurement. Finally, after eliminating circuits having a resonance frequency which risks to disturb the measurement, there are several possible circuits. These circuits are represented with an underlined title in Fig. 14. Measurements presented in this paper have been performed with the method "UPS", i.e, the Agilent power supply is powered thanks to batteries and there is no coils and no amplifier. Although the attenuation is higher than other circuits, this is the simplest system to operate, the only drawback is the short lifetime of batteries before recharging them.

B. Measurements

Measurements have been performed with the second configuration of the probe, see Fig. 4. The probe has been placed near the channel axis and X-direction step by step measurements have been performed with a step size of X=10 mm. The signal has been recorded during 0.16 s with a resolution of 20 ns and a sample rate of 50 MS/s. Figure 15 (left-hand side) shows a typical raw signal corresponding to the plasma potential (AC signal only) as a function of time. Fourier Transform (FT) has been performed on each signal. Figure 15 (right) shows the evolution of the FT of the signal when the probe moves closer to the thruster. The frequency ranges of the BM and the ITT oscillations are clearly seen. Although no frequency oscillation was forced during the recording, the BM presents the maximum amplitude at 18 kHz. In the frequency range of the ITT, there are two structures. A low frequency structure is composed of several peaks. Typically three peaks are present. They have a narrower frequency range when the probe moves closer to the thruster. For x = 12 cm, the frequencies of these peaks are 70, 150, 250 kHz (the last one has a lower amplitude). For x = 3 cm, the first peak shifts to 110 kHz. The higher frequency structure is a sharp peak at 350 kHz with a constant frequency whatever the position of the probe. These two structures certainly do not correspond to the same physical phenomenon.

V. Conclusion

In this contribution, time-averaged measurements with an emissive probe of V_p, V_f, T_e and $\vec{E}$ performed in the near-field plume of a low power Hall thruster are presented. A fast linear drive has been used to avoid the sputtering of the probe near the thruster exit plan. In order to be able to probe high frequency oscillations of the plasma, several electronic circuits have been tested. Time-resolved measurements in the far-field plume are presented, showing the spatial evolution of the breathing mode and the ion transit time oscillation. In the near-future, time-averaged contour plots will be performed for several channel geometries and materials, thruster powers and B field topologies in order to understand the influence of these parameters on plasma properties. Furthermore, a time-resolved acquisition system has been built to probe high frequency oscillations. It will be used to obtain changes of plasma parameters versus time and position.

Acknowledgments

A. Pétin benefits from a PhD grant from the French Ministery of Sciences.

References

Dannenmayer, K., Kudrna, P., Tichý, M., and Mazouffre, S. (2012). Time-resolved measurement of plasma parameters in the far-field plume of a low-power hall effect thruster. *Plasma sources Sci. Technol.*, 21(055020).

Dannenmayer, K. and Mazouffre, S. (2011). Elementary scaling relations for Hall effect thruster. *J. Propulsion Power*, 27(236).

Dannenmayer, K. and Mazouffre, S. (2012). Compact high-speed reciprocating probe system for measurements in a Hall thruster discharge and plume. *Rev. Sci. Instrum.*, 83(123503):1–5.

Dannenmayer, K. and Mazouffre, S. (2013). Electron flow properties in the far-field plume of a Hall thruster. *Plasma sources Sci. Technol.*, 22(035004).

Mazouffre, S., Bourgeois, G., Dannenmayer, K., and Lejeune, A. (2012). Ionization and acceleration processes in a small, variable channel width, permanent-magnet Hall thruster. *J. Phys. D: Appl. Phys.*, 45(185203):1–7.

Sheehan, J. P. and Hershkowitz, N. (2011). Emissive probes. *Plasma Sources Sci. Technol.*, 20(1-2):1–22.

Smith, A. W. and Cappelli, M. A. (2010). Time and space-correlated plasma potential measurements in the near field of a coaxial Hall plasma discharge. *Phys. Plasmas*, 16(073504).

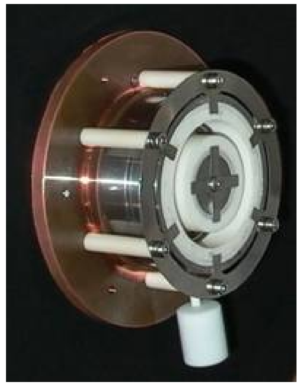

Figure 1. Picture of the 200 W-class PPI Hall thruster

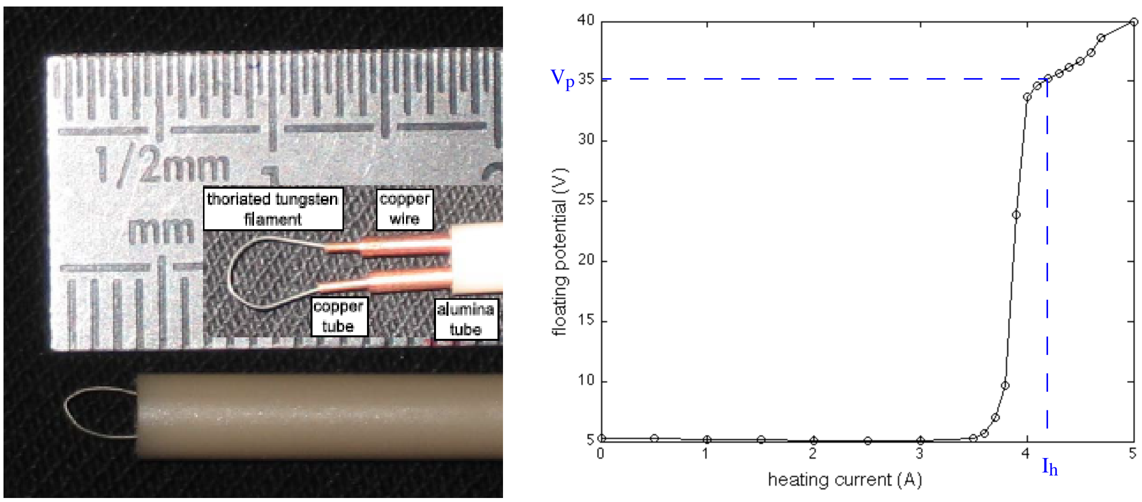

Figure 2. Left: picture showing the building of the emissive probe. Right: heating curve of an emissive probe showing the saturation of the floating potential of the probe. In practice, the probe potential continues to increase and the heating current I_h is chosen just after the knee of the curve.

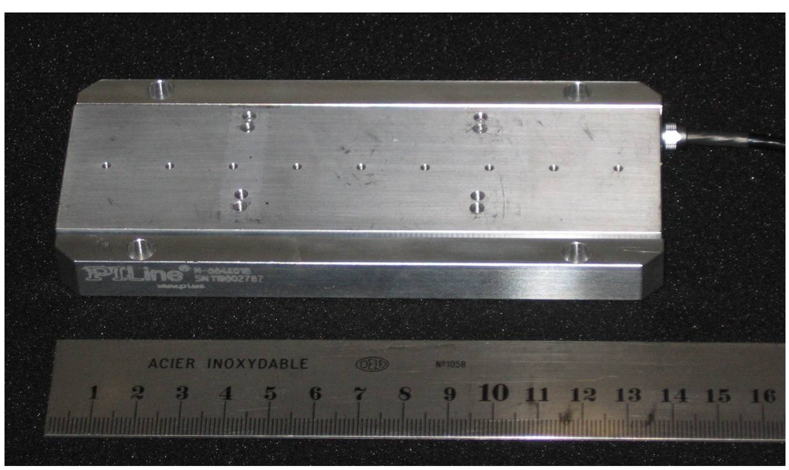

Figure 3. Picture of the piezoelectric translation stage

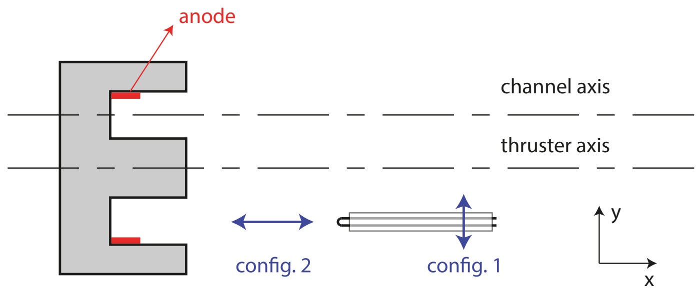

Figure 4. Scheme showing the configurations of the probe. The probe is parallel to the thruster axis. The movement of the linear drive is, in the "config. 1" in the Y-direction, and in the "config. 2" in the X-direction. In the "config. 1", the thruster (in grey) has also a step by step movement in the X-direction.

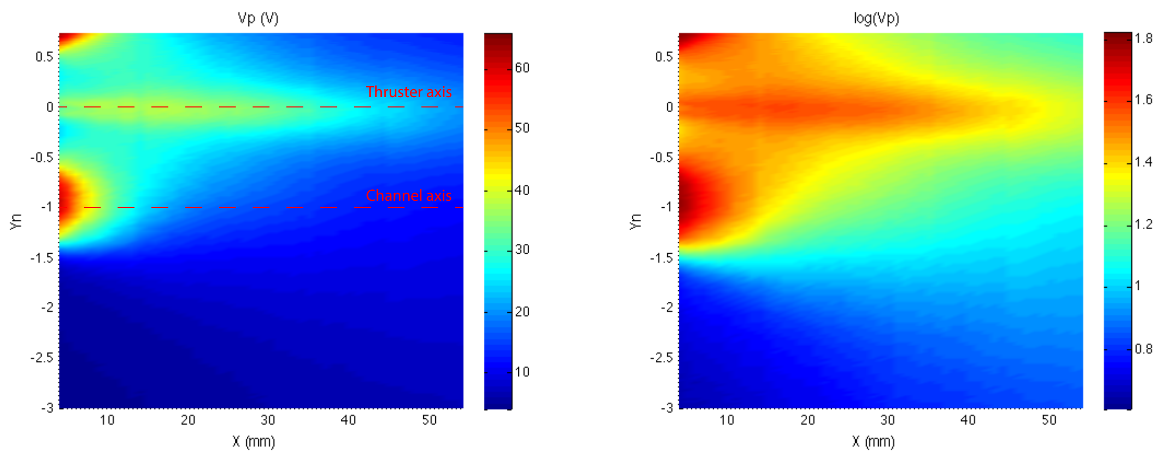

Figure 5. Contour plot of the plasma potential (top) and the decimal logarithm of the plasma potential (bottom) in the near field plume of the PPI hall thruster. The thruster operating parameters are I_d =0.93-0.94 A, U_d=200 V, $\dot{m}_{Xe}$=1 mg/s and the pressure is p=1.2 10^{-4} mbar-N_2.

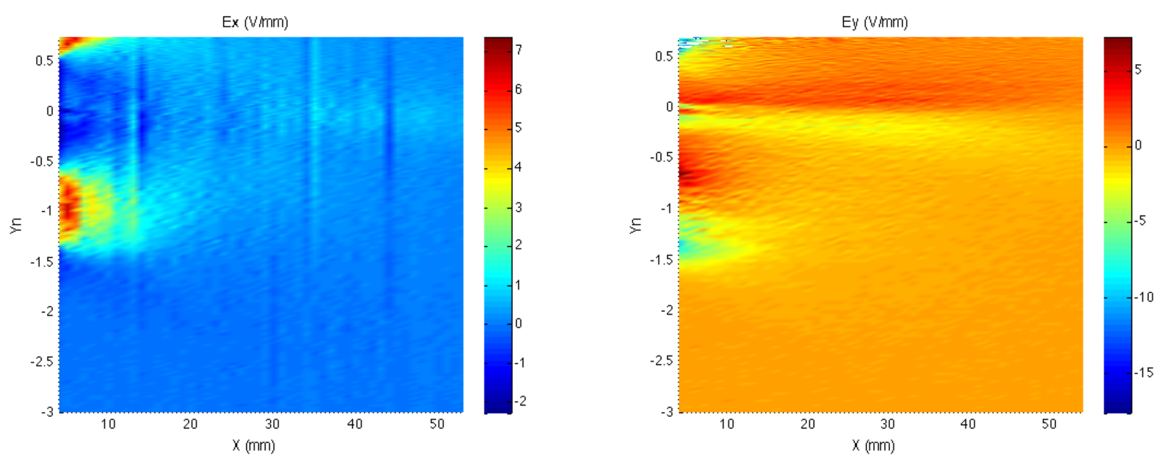

Figure 6. Contour plot of the x-component (top) and the y-component (bottom) of the electric field (V/mm) in the near field plume of the PPI hall thruster. The thruster operating parameters are I_d =0.93-0.94 A, U_d=200 V, $\dot{m}_{Xe}$=1 mg/s and the pressure is p=1.2 10^{-4} mbar-N_2.

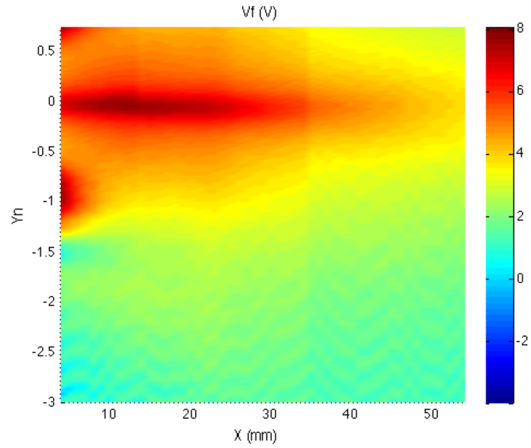

Figure 7. Contour plot of the floating potential (V) in the near-field plume of the PPI hall thruster. The thruster operating parameters are I_d =0.93-0.94 A, U_d=200 V, $\dot{m}_{Xe}$=1 mg/s and the pressure is p=1.2 10^{-4} mbar-N_2.

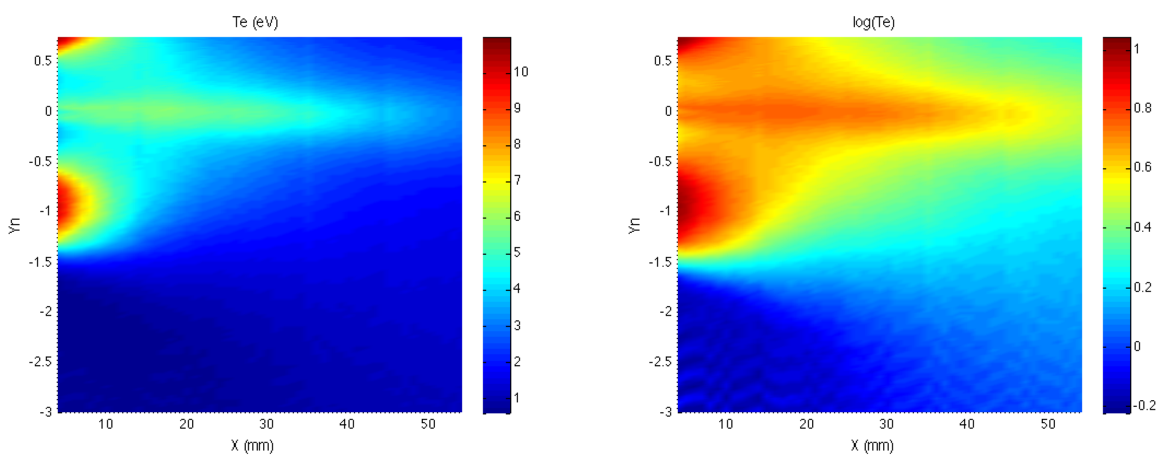

Figure 8. Contour plot of the electron temperature (eV) and the decimal logarithm of the electronic temperature in the near field plume of the PPI hall thruster. The thruster operating parameters are I_d =0.93-0.94 A, U_d=200 V, $\dot{m}_{Xe}$=1 mg/s and the pressure is p=1.2 10^{-4} mbar-N_2.

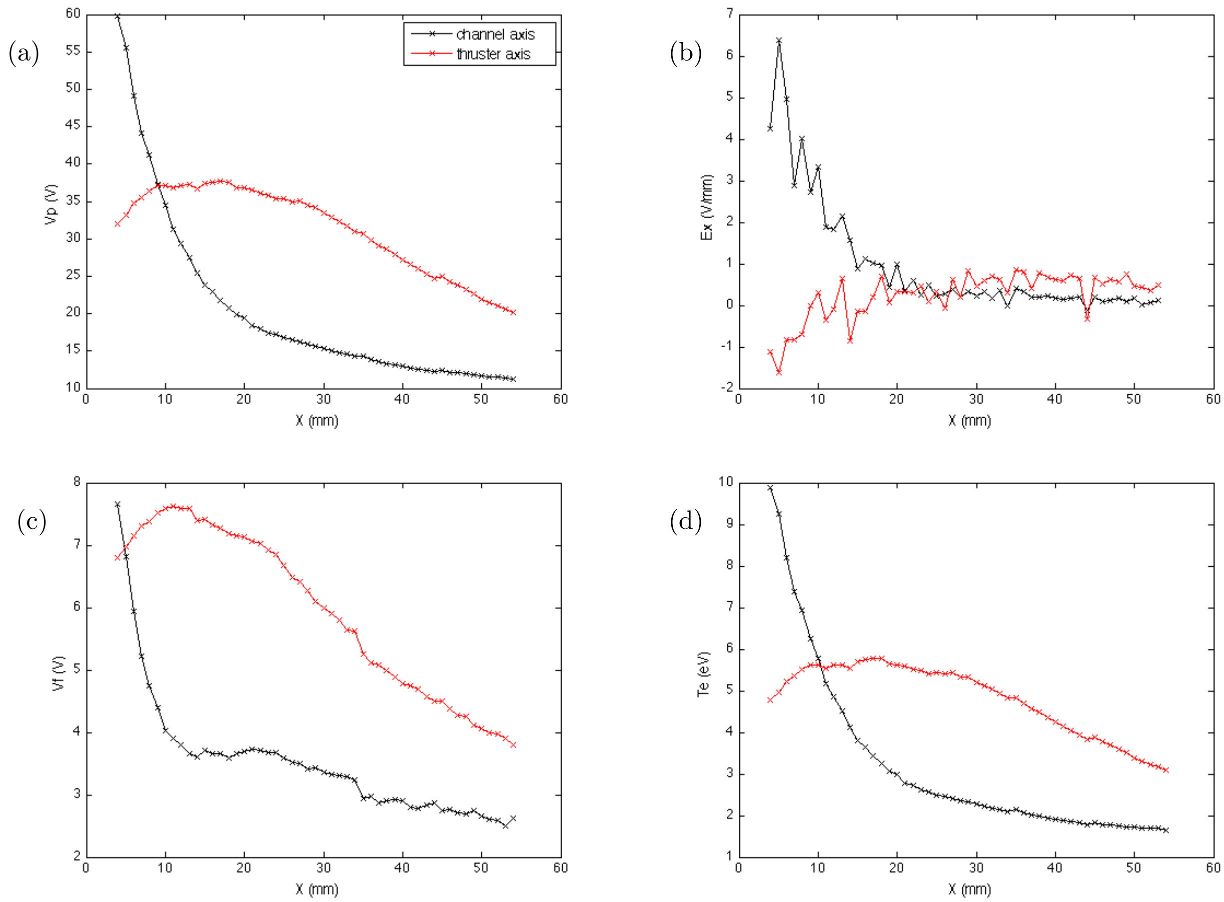

Figure 9. Profiles of a) V_p, b) E_x, c)V_f, d)T_e in function of the distance to the thruster. The black curve corresponds to the channel axis and the red curve to the thruster axis. The thruster operating parameters are I_d =0.93-0.94 A, U_d=200 V, $\dot{m}_{Xe}$=1 mg/s and the pressure is p=1.2 10^{-4} mbar-N_2.

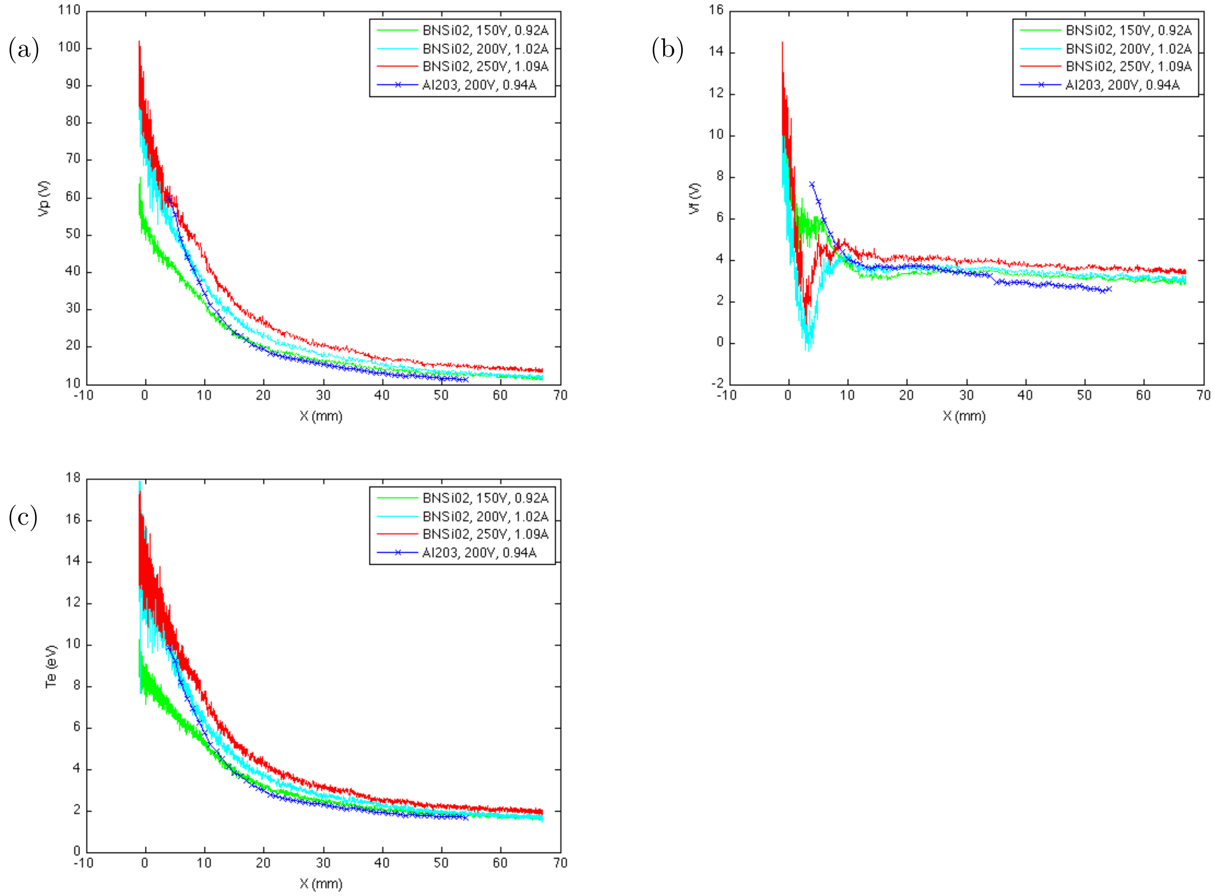

Figure 10. a) plasma potential, b) floating potential, c) electron temperature versus the distance from the thruster exit plan (X=0). For each graph, three voltages (150, 200, 250 V) are plotted in case of the channel ceramic BNSi0_2 and one voltage 200 V for Al_20_3.

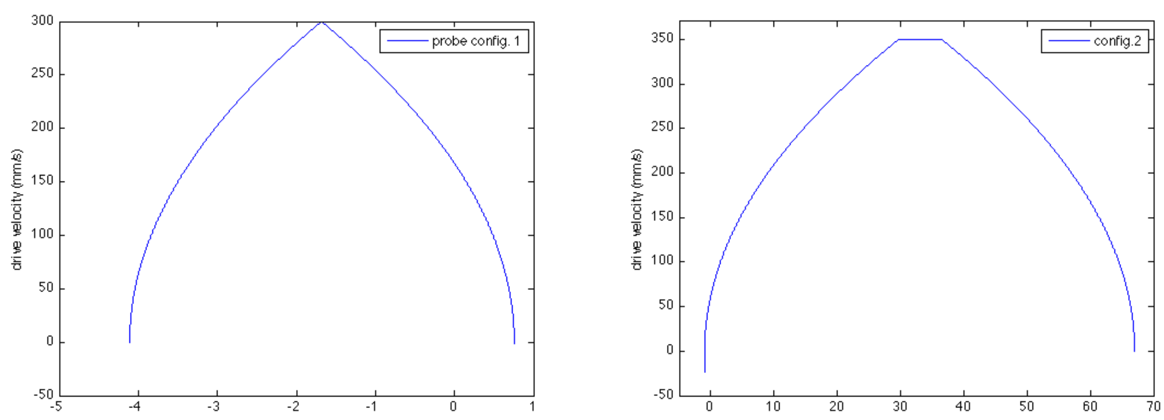

Figure 11. On left side: probe velocity versus Y-direction for the first probe configuration. On right side: probe velocity versus X-direction for the second probe configuration.

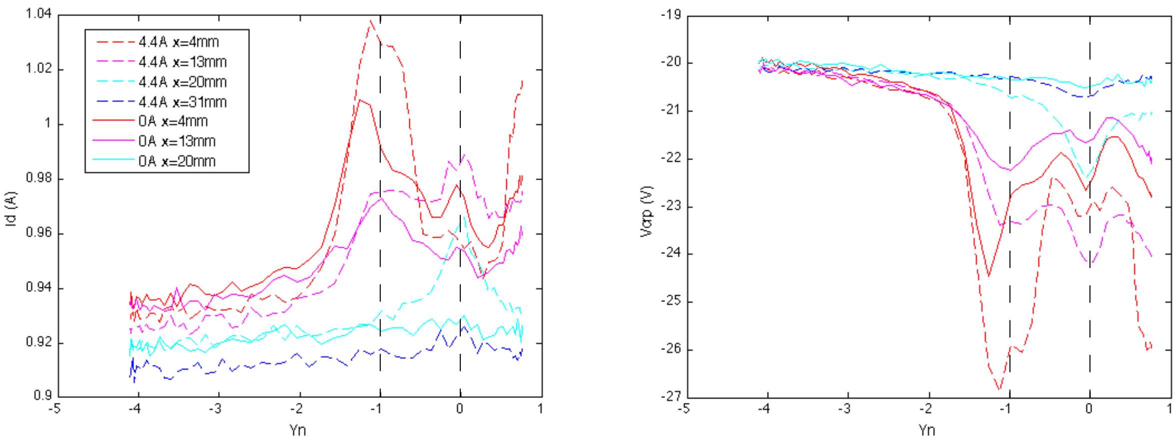

Figure 12. On left side: I_d versus Y-direction. On right side: V_{crp} versus Y-direction. In each graph, the heated ("4.4 A") and cold ("0 A") probe disruptions are compared, for several distances from the thruster plan (x=0).

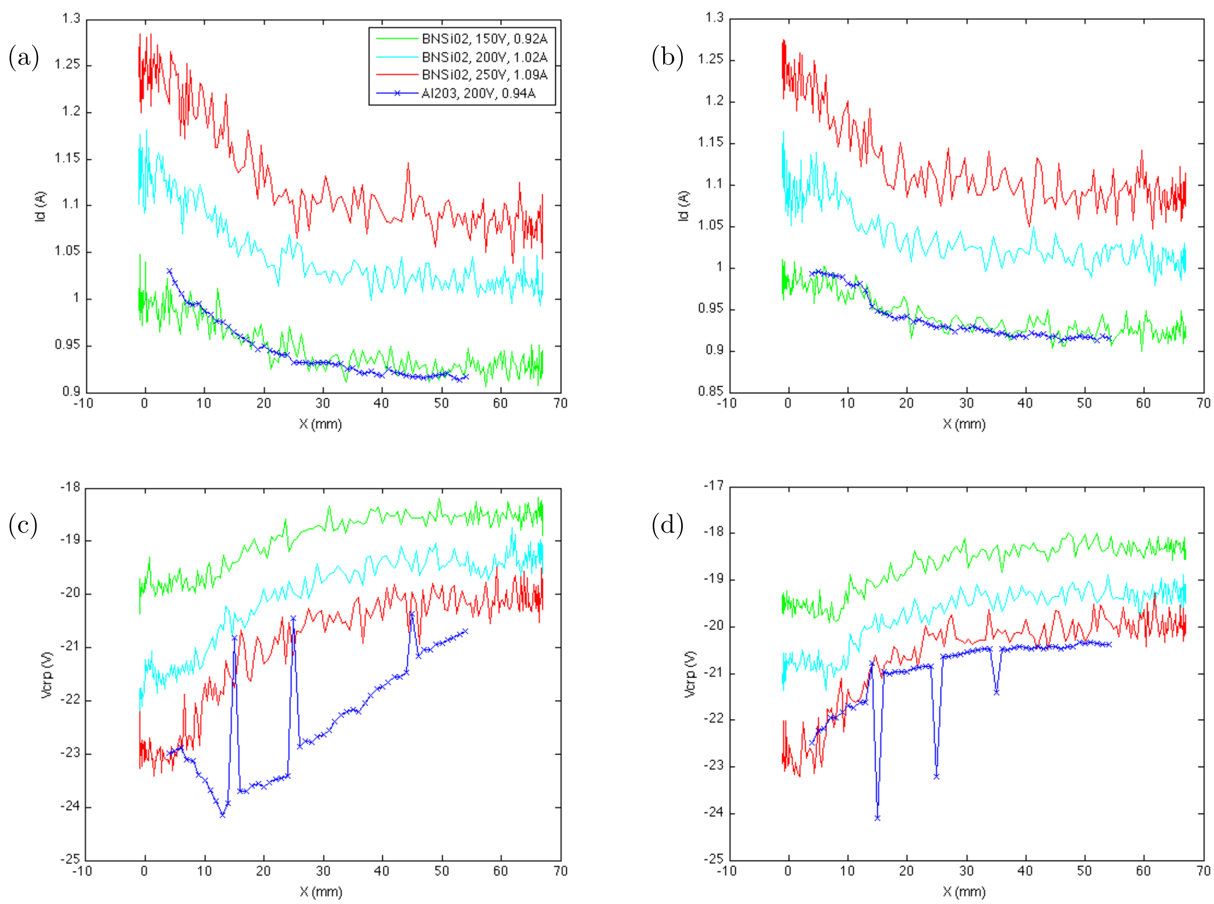

Figure 13. I_d versus the distance from the truster axis (X=0) in case of a) a heated probe, b) a cold probe. V_{crp} versus the distance from the truster axis (X=0) in case of c) a heated probe, d) a cold probe. These profiles are given for channel axis. For each graph, three voltages (150, 200, 250 V) are plotted in case of the internal channel ceramic $BNSi0_2$ and one voltage 200 V for Al_20_3.

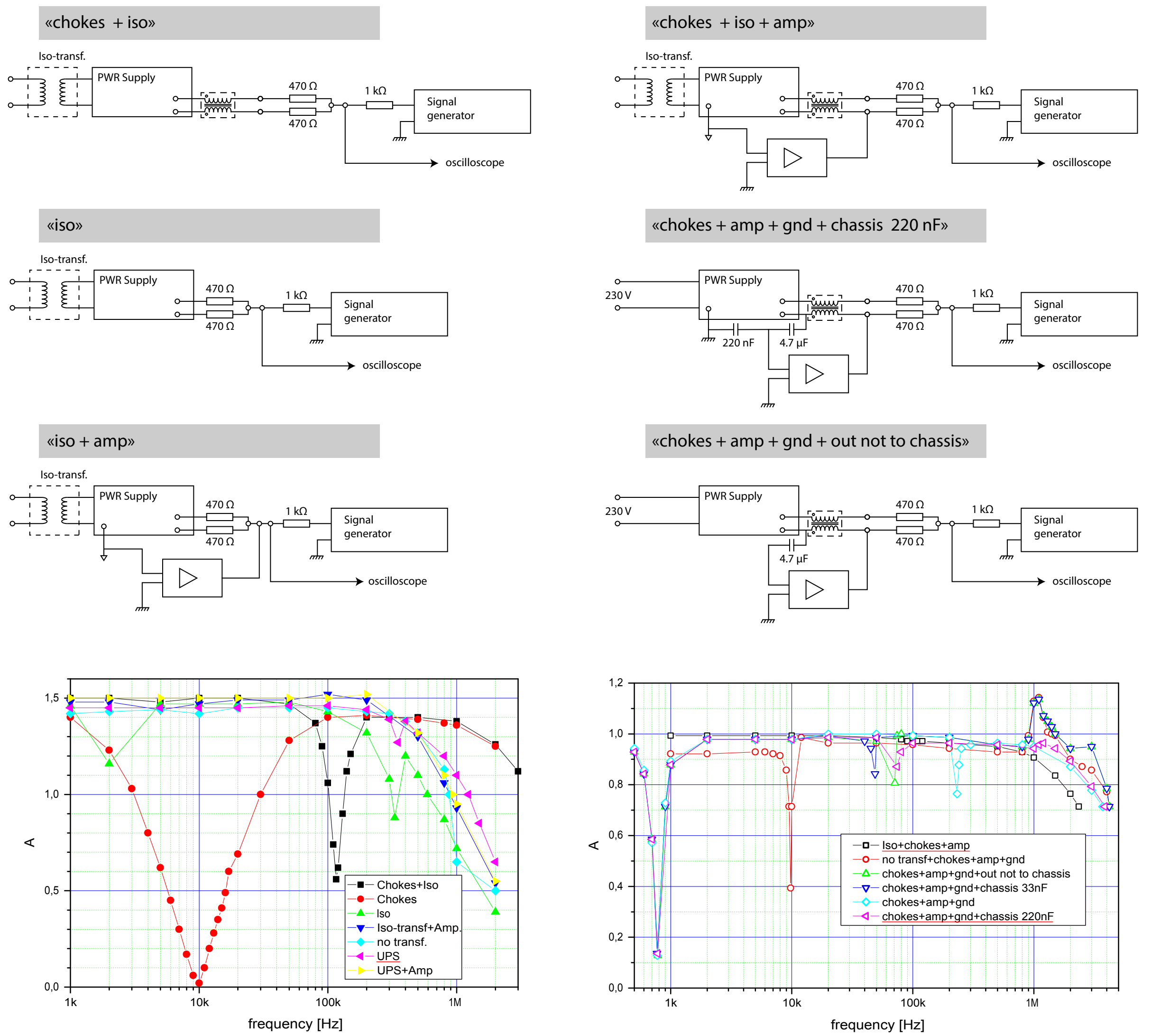

Figure 14. Top: Main tested circuits. Bottom: amplitude of transfer functions for each tested circuit. Some circuits are not sketched but are easy to derive from the main ones.

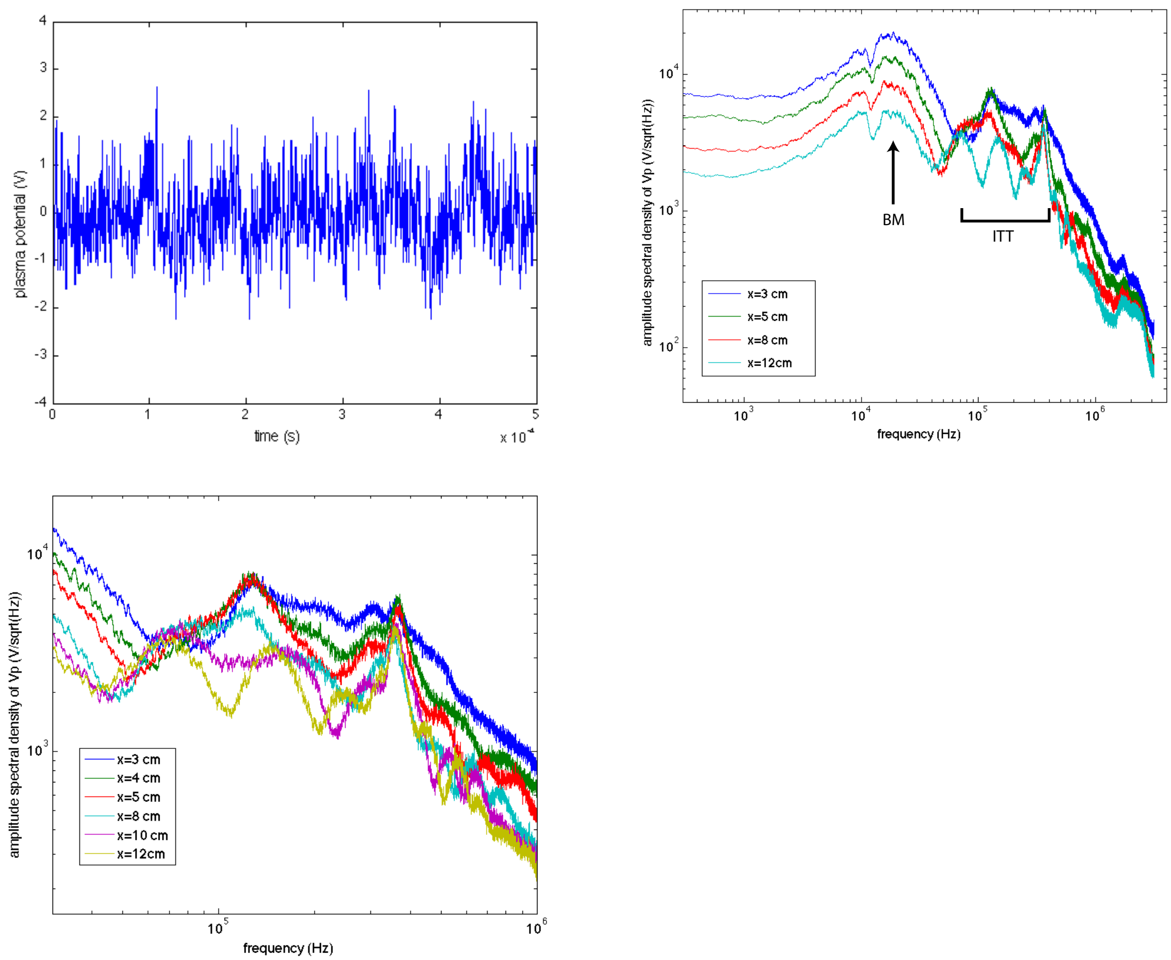

Figure 15. Top, on left side: raw data V_p versus time for Y near the channel axis and X=3 mm. Top, on right side: FT of V_p recorded for several X positions. Bottom: Behavior of FT (V_p) for more probe positions.